Author Manuscript

Evidence for Magnetic Reconnection as the Precursor to Discrete Aurora at Mars

C.F. Bowers[1], G.A. DiBraccio[2], J.A. Slavin[1], B. Johnston[3], N.M. Schneider[3], D. A. Brain[3], A. Azari[4]

[1]University of Michigan, Department of Climate and Space Sciences and Engineering, Ann Arbor, MI
[2]NASA Goddard Spaceflight Center, Greenbelt, MD
[3]University of Colorado/Laboratory for Atmospheric and Space Physics Boulder, CO
[4]University of California Berkeley, Space Sciences Laboratory, Berkeley, CA

Key Points:

- Discrete aurora over two regions of crustal fields at Mars occur under specific draped magnetic field conditions
- Of the 49 discrete aurora analyzed, 42 (86%) occur under conditions that favor anti-parallel magnetic reconnection
- Reconnection plays a role in discrete aurora onset, explaining trends in auroral detections including local time and upstream conditions

This is the author manuscript accepted for publication and has undergone full peer review but has not been through the copyediting, typesetting, pagination and proofreading process, which may lead to differences between this version and the Version of Record. Please cite this article as doi: 10.1029/2023JA031622.

This article is protected by copyright. All rights reserved.

Author Manuscript

Abstract

Discrete aurora at Mars are characterized as localized, short-lasting ultraviolet emissions on the nightside. They are caused by the precipitation of accelerated electron along open magnetic field lines and their collision with the Martian atmosphere. Discrete auroral emissions detected by the Imaging Ultraviolet Spectrograph (IUVS) instrument onboard the Mars Atmosphere and Volatile EvolutioN (MAVEN) spacecraft occur most frequently over the strongest crustal magnetic anomalies at Mars and under particular local time and upstream interplanetary magnetic field (IMF) conditions. These trends suggest that the onset of discrete aurora is controlled by the processes that govern the interaction between the draped IMF and the crustal magnetic anomalies. Here, we analyze MAVEN magnetometer measurements over regions of strong crustal fields during 49 discrete auroral events observed by IUVS. Our results indicate that the draped IMF orientations during each discrete auroral event show a clear tendency to be anti-parallel to the underlying crustal anomaly magnetic fields near the location of the emission onset. This suggests that magnetic reconnection, a process that favors anti-parallel magnetic field regimes, between the crustal fields and the draped IMF plays a role in discrete aurora formation. Of the 49 discrete auroral events analyzed, 42 (86%) occurred under draped IMF conditions that are susceptible to reconnection with the underlying crustal anomalies. This investigation produces strong evidence linking discrete aurora to magnetic reconnection at Mars and provides insights into other trends in discrete auroral activation such as local time and upstream IMF conditions.

Plain Language Summary

There are regions on the surface of Mars that possess strong magnetic fields. Ultraviolet aurora known as "discrete aurora" at Mars are observed most frequently over a region of these strong crustal fields and are caused by the energetic collision between charged particles and the Martian atmosphere. These particles are thought to be the result of the interaction between Martian magnetic fields and the flow of charged particles and interplanetary magnetic field (IMF) known as the solar wind. Our work analyzes magnetic field observations from the magnetometer onboard the Mars Atmosphere and Volatile EvolutioN (MAVEN) spacecraft along orbits in which discrete aurora were detected over a region of strong crustal magnetism. We find that discrete auroral emissions over these strong crustal magnetic fields occur most frequently when the surrounding draped IMF conditions are susceptible to undergoing a process called "magnetic reconnection," in which magnetic field lines are reassigned into a different magnetic connectivity. This is the first study to definitively link the process of discrete aurora to magnetic reconnection and provides a framework for understanding previously unexplained trends in discrete aurora activation at Mars.

1 Introduction

Auroral emissions are created when precipitating particles travel along magnetic field lines and excite fluorescence in the neutral atmosphere through collisions. At Mars, the localized crustal fields provide a magnetic pathway for these precipitating particles (Acuña et al., 1999). Martian auroral emissions were first observed by the Spectroscopy for the Investigation of the Characteristics of the Atmosphere of Mars (SPICAM) instrument onboard the Mars Express spacecraft (e.g., Bertaux et al., 2005; Leblanc et al., 2006). Since then, the Mars Atmosphere and Volatile EvolutioN (MAVEN) spacecraft (Jakosky et al., 2015), which arrived at Mars in September 2014, has observed auroral phenomenon through data collected by the Imaging Ultraviolet Spectrograph (IUVS) instrument (McClintock et al., 2015). Dis-

This article is protected by copyright. All rights reserved.

Author Manuscript

crete aurora are characterized by localized, short-lived ultraviolet (UV) emissions on the nightside of Mars (Schneider et al., 2018). The locations of these discrete auroral emissions are correlated with the underlying radial crustal field strength, with discrete aurora occurring most frequently over the region of strongest crustal magnetism in the southern hemisphere which is centered at ∼180°E longitude (Schneider et al., 2021). We note discrete aurora are fundamentally distinct from both proton auroral emissions (e.g., Deighan et al., 2018; Hughes et al., 2019) and diffuse auroral emissions (Schneider et al., 2015), which are dispersed globally and span up to thousands of kilometers across the surface.

Discrete auroral emissions are also closely associated with downward electron acceleration events (e.g., Brain et al., 2006; Gérard et al., 2015; Xu et al., 2020). These accelerated electrons are the source for discrete auroral emissions, and also are observed most frequently over the strongest crustal anomalies (Halekas et al., 2008), particularly over regions in which the crustal magnetic fields are open, with one end of the magnetic field line connected to the planet and the other end connected to the interplanetary magnetic field (IMF) (e.g., Schneider et al., 2021; Fang et al., 2022). Open magnetic field lines allow solar wind particles to access the neutral atmosphere. Both modeling (e.g., Soret et al., 2016, 2021) and empirical (Xu et al., 2022) studies have analyzed the precipitating electrons traveling along these open fields that ultimately produce discrete aurora emissions, known as auroral electrons. Soret et al. (2021) determine that auroral electrons require energies > 50 eV to ultimately produce discrete auroral emissions that are detectable by the IUVS or SPICAM instruments. This energy level is higher than the nominal electron energy within the nightside of Mars, suggesting an acceleration mechanism within the magnetosphere of Mars is required to produce auroral electrons.

Recent studies of discrete auroral emissions with IUVS limb scans (spectra taken near periapsis looking transverse to the planet) have revealed trends in auroral emissions with magnetospheric conditions. Schneider et al. (2021) found that discrete auroral emissions observed via limb scan observations over the region of strong crustal magnetism show a preference for duskward upstream IMF orientations and evening local time (LT) hours (∼1800-2200). Thus, discrete aurora activation depends on both the upstream IMF orientation and the strength/position of the crustal magnetic fields. This implies that discrete auroral emissions at Mars are the result of "mini-magnetospheric" interactions between the crustal anomalies and the draped IMF, analogous to auroral signatures in an atmosphere contained within an intrinsic magnetosphere (Angelopoulos et al., 2008). The interaction between the draped IMF and the crustal fields may generate a variety of local acceleration mechanisms summarized in Brain and Halekas (2012), including wave-particle interactions (e.g., Fowler et al., 2020, 2021), narrow electrostatic potential layers, similar to the inverted-V electron acceleration signatures observed over auroral arcs at Earth (e.g., Brain et al., 2006; Xu et al., 2020), magnetotail current sheets (Halekas et al., 2008), and magnetic reconnection (e.g., Brain et al., 2006; Cravens et al., 2020; Harada et al., 2020). However, the precise magnetospheric processes that play a role in discrete aurora at Mars have been difficult to identify.

A strong candidate magnetospheric process that enables discrete aurora formation is magnetic reconnection between the draped IMF and the crustal anomalies at Mars. Reconnection is thought to play a role in discrete aurora at magnetized objects such as Earth (e.g., Frey et al., 2003; Frey, 2007; Angelopoulos et al., 2008) and Ganymede (e.g., McGrath et al., 2013; Ebert et al., 2022). The process of magnetic reconnection generates open magnetic fields that connect to the higher altitude ionosphere, magnetosheath, and draped magnetotail. Kinetic simulations have found open field lines at Mars also naturally generate electric potential structures that accelerate electrons downward (Poppe et al., 2021). Therefore, magnetic reconnection

This article is protected by copyright. All rights reserved.

Author Manuscript

between the crustal fields and the IMF may act as a precursor to discrete aurora by creating the open field lines that subsequently form the potentials that generate auroral electrons. Magnetic reconnection between the crustal anomalies at Mars and the draped IMF produces byproducts that have been observed throughout the magnetosphere of Mars, including Hall magnetic fields (Eastwood et al., 2008), ion jets (e.g., Harada et al., 2020; Cravens et al., 2020), flux ropes (e.g., Cloutier et al., 1999; Brain et al., 2010; Hara et al., 2014; Bowers et al., 2021), and open magnetic topology (e.g., Brain et al., 2007, 2020; Dubinin et al., 2008; R. Lillis et al., 2011; Xu et al., 2014, 2017; Weber et al., 2017).

In this study, we use MAVEN magnetospheric data to explore the hypothesis that magnetic reconnection plays a major role in the onset of discrete auroral formation at Mars (hereafter referred to as the "reconnection hypothesis"). Reconnection is a localized process that depends heavily on the magnetospheric conditions and relative orientation of the underlying crustal magnetic fields. With this in mind, our analysis focuses on previously reported discrete auroral events detected over the strong crustal anomaly region (37°S – 68°S latitude, 155°E – 211°E longitude) via nadir scans captured by the IUVS instrument onboard MAVEN described in the companion to this paper: Johnston et al. (2023), hereafter referred to as Johnston23. We analyze this region from a mini-magnetospheric point of view. Specifically, we compare the draped IMF orientations during the onset of discrete aurora with the orientations of the underlying crustal fields as measured by the MAG instrument onboard MAVEN (Connerney et al., 2015). We then create magnetic maps of the nominal draped IMF conditions around Mars to elucidate the conditions that give rise to discrete aurora emissions, including draped field orientation, local time, and upstream IMF orientation. Our results strongly support the reconnection hypothesis and provide new insights into previously unexplained magnetospheric trends in discrete auroral emission and auroral electron fluxes surrounding this strong crustal field region.

2 Observations and Methodology

2.1 Instrumentation and Observations

We investigate the magnetospheric conditions surrounding discrete auroral emissions through an analysis of data provided by the MAVEN spacecraft. MAVEN's orbit precesses around the planet and provides global coverage of the Mars atmosphere and space environment with apoapsis reaching out to ∼6200 km altitude and periapsis ∼150 km altitude. We analyze the magnetic field environment of Mars using data provided by the MAG instrument (Connerney et al., 2015) which measures vector magnetic fields at a maximum sampling rate of 32 vectors/s. The magnetic field measurements are analyzed in the Mars Solar Orbital (MSO) coordinate system, $[\hat{X}_{MSO},\hat{Y}_{MSO},\hat{Z}_{MSO}]$. We also analyze magnetic field measurements in the planetary coordinate system $[\hat{R},\hat{E},\hat{N}]$, in which $\hat{R}$ points radially outward from Mars, $\hat{E}$ points towards geographic east, and $\hat{N}$ points towards geographic north.

To investigate the relationship between discrete auroral emissions and upstream IMF conditions, we utilize in situ and proxy information of the upstream solar wind. The Solar Wind Ion Analyzer (SWIA) (Halekas et al., 2015) instrument measures the properties of the solar wind and covers an energy range of 25 eV to 25 keV at cadences up to 4 s. To estimate the IMF orientation during auroral emissions, we identify orbits in this data set in which MAVEN directly measured the pristine solar wind using both SWIA and MAG measurements in a process developed by Halekas et al. (2017). Due to the orbital geometry of MAVEN during these nightside apoapsis passes, many orbits do not enter the solar wind and cannot directly measure the IMF orientation. Plasma conditions in the magnetosheath, such

This article is protected by copyright. All rights reserved.

Author Manuscript

as velocity and magnetic field orientation, depend on the upstream orientation of the IMF (Halekas et al., 2017), and so we expect the magnetosheath to retain information regarding the upstream IMF conditions. We therefore augment the catalog of in situ solar wind measurements with a proxy estimate for the IMF using a technique described in Ruhunusiri et al. (2018), which implements an artificial neural network to estimate upstream solar wind conditions from MAVEN measurements taken within the magnetosheath. Ruhunusiri et al. (2018) trained this neural network on MAVEN orbits that sampled both the magnetosheath and the solar wind, taking into account both plasma (density, temperature, speed) and magnetic field data of both regimes. We note that Ruhunusiri et al. (2018) took steps to minimize the time delay between the magnetosheath measurement and the associated solar wind measurement used to train the model.

The discrete aurora data set was compiled via spectra collected by the IUVS instrument onboard MAVEN (McClintock et al., 2015). In this study, we utilize the event list of discrete aurora observations at Mars reported by Johnston23. This data set is comprised entirely of nadir scans (spectra taken near apoapsis looking back towards the nightside of Mars), as opposed to limb scan observations of discrete aurora described in Schneider et al. (2021). The geometry of nadir viewing provides the necessary spatial resolution to accurately place events on the crustal field map. To form this data set, Johnston23 first visually inspected nadir scans of Mars to identify emissions in the mid-ultraviolet range. Then, they compared the spectra observed from IUVS to a CO Cameron band template and performed a linear regression analysis to compare the two spectra. A Pearson-R correlation was then performed between the CO Cameron band template and the observed auroral spectrum; emissions with a Pearson-R value greater than 0.6 (Schneider et al., 2021) were classified as discrete auroral observations and are added to the data set. This procedure identified 126 discrete aurora events on the nightside of Mars from 5896 MAVEN orbits.

2.2 Overview of Auroral Events

Johnston23 determined the geographic location of the discrete auroral emission source for each event in their database by analyzing the emission angle of the discrete auroral signature together with the ephemeris (latitude, longitude, altitude) data of the spacecraft at the time of the discrete auroral observation. A single discrete auroral emission detection can span up to $\sim$ 30 pixels on the IUVS detector in nadir viewing images, and therefore may extend up to to $\sim$ 1500 km on a geographic map. Given the spatial extent of each auroral detection provided by the database of events in Johnston23, we calculate the "spatial center" by averaging the latitude/longitude location of every pixel associated with each discrete aurora detection within this database.

We then plot the spatial center of each discrete auroral observation over a data-derived map of the radial field strength of the crustal anomalies (Figure 1). This map of crustal anomaly strength and orientation is formed by compiling MAVEN MAG low-altitude ($<$ 1000 km) measurements into 1° longitude by 1° latitude bins and separated into 200 km altitude ranges (200-400 km, 400-600 km (Figure 1), and 600-800 km). The details of this process are described by Weber (2020) and the database has been updated for this study to include MAVEN measurements through March 2022. Due to MAVEN's orbital inclination, there are limited measurements near the poles, and therefore, the crustal map only extends from 75°S – 75°N latitude. The discrete auroral events tend to cluster around the strongest crustal anomaly region in the southern hemisphere at $\sim$ 180° E. longitude, which is consistent with limb-scan studies of auroral observations reported in Schneider et al. (2021) and trends with precipitating auroral electron fluxes (e.g.,

This article is protected by copyright. All rights reserved.

Author Manuscript

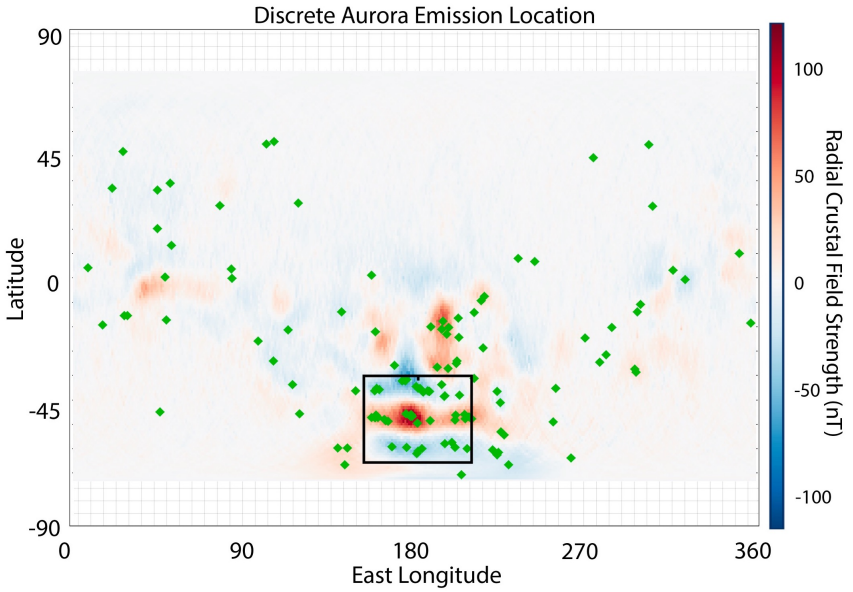


Figure 1. Map of crustal magnetic fields at Mars generated from MAVEN passes from 2014-2022 at altitudes ranging from 400-600 km colored by the radial magnetic field strength. Each green diamond represents the spatial center of a discrete auroral emission detected by IUVS via nadir scans of the nightside of Mars. Adapted from Johnston23 using MAVEN MAG data.

Brain et al., 2006; Xu et al., 2022). To investigate this trend from a magnetospheric point of view, we turn our attention to the discrete auroral events that occur within this strong crustal field region.

Figure 2 is a zoomed-in version of Figure 1 centered in the southern hemisphere over some of the strongest crustal anomalies at Mars ($|B|$ exceeds 1000 nT between 150 km-200 km in altitude) stretching from –34°S to –68°S in latitude and 155°E to 211°E in longitude. We also plot the transverse (non-radial) component of the crustal fields represented as black arrows. This region will be referred to as R_f for the remainder of this paper. R_f consists of three regions dominated by radial crustal magnetic fields: a radially outward region at the center ($\sim$ 50°S) bracketed by two radially inward regions with one located to the north ($\sim$ 38°S) and the other to the south ($\sim$ 65°S). The northern (southern) radially inward region is connected to the central radially outward region via transverse crustal fields that close northward (southward). Thus, R_f can be simplified into two crustal anomalies: a northern anomaly that closes to the north and a southern anomaly that closes to the south. These anomalies form two mini-magnetospheres (also referred to as "magnetic arcades" in Johnston23 due to their linear structure) under the influence of the downward pressure from the solar wind in the magnetosheath. They are separated vertically on the crustal anomaly map, close magnetically in opposite directions, and protrude from the surface and interact with the draped IMF.

We define the northern mini-magnetosphere to lie between 52°S and 37°S outlined by the grey box, and the southern mini-magnetosphere to lie between 68°S and 52°S outlined by the yellow box (Figure 2a). Of the 126 discrete auroral events, 49 occur within R_f with 34 occurring within the grey box that defines northern mini-magnetosphere, and 15 occurring within the yellow box the defines the southern mini-magnetosphere. These 49 discrete auroral events were observed along 32 unique orbits. While Figure 2 shows the anomalies at the altitude range from

This article is protected by copyright. All rights reserved.

Author Manuscript

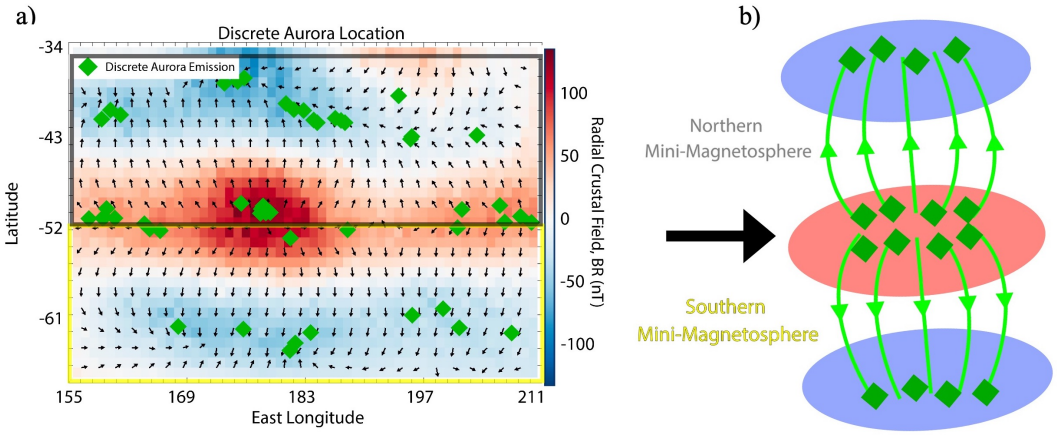


Figure 2. a) Zoomed-in map of data-derived crustal magnetic fields within R_f colored by the radial crustal field strength. The black arrows represent the transverse orientation of the crustal fields. Each green diamond represents the spatial center of a discrete auroral emission detected by IUVS via nadir scans of the nightside of Mars. The grey/yellow boxes approximately represent the northern/southern anomaly region. b) Schematic representation of the two "mini-magnetospheres" that comprise R_f where red/blue represent radially outward/inward regions, and light green arrows represent the transverse fields that characterize the orientations of the northern and southern anomalies.

400 – 600 km, we note these anomalies retain their structure up to altitudes of ∼ 1400 km (not shown here). The location of the events in Figure 2 demonstrates a clear spatial trend, where discrete auroral emissions occur mainly over the regions with radially oriented magnetic fields (i.e. cusps) of this crustal field region, consistent with previous discrete aurora studies (Schneider et al., 2021). That is, the discrete auroral emissions tend to cluster around the footprints of the two crustal field mini-magnetospheres that comprise R_f. We note that the radially outward region dividing the two boxes is magnetically connected to both the northern mini-magnetosphere and the southern mini-magnetosphere whereas the radially inward regions to the north and south are also connected magnetically to surrounding crustal anomalies.

2.3 Draped Field Orientation and the Reconnection Hypothesis

Magnetic reconnection is a process that favors an anti-parallel magnetic field configuration. Therefore, if the reconnection hypothesis outlined in Section 1 is correct, then we would expect the onset of discrete aurora within R_f to favor certain draped IMF orientations, determined by the orientation of the underlying crustal mini-magnetosphere. For example, given the northward-and southward- directed mini-magnetospheres illustrated in Figure 2b, a southward draped IMF would be anti-parallel to the northern mini-magnetosphere (Figure 3a). In comparison to the southern mini-magnetosphere, the northern mini-magnetosphere is therefore more susceptible to undergoing magnetic reconnection with a southward draped IMF.

In this scenario, reconnection "opens-up" the closed crustal fields of the northern mini-magnetosphere to solar wind plasma. These open fields generate potential structures that may accelerate electrons to the high energies associated with auroral electrons (Poppe et al., 2021). Auroral electrons would then precipitate towards the planet and deposit their energy into the atmosphere over the footprints of the north-

This article is protected by copyright. All rights reserved.

Author Manuscript

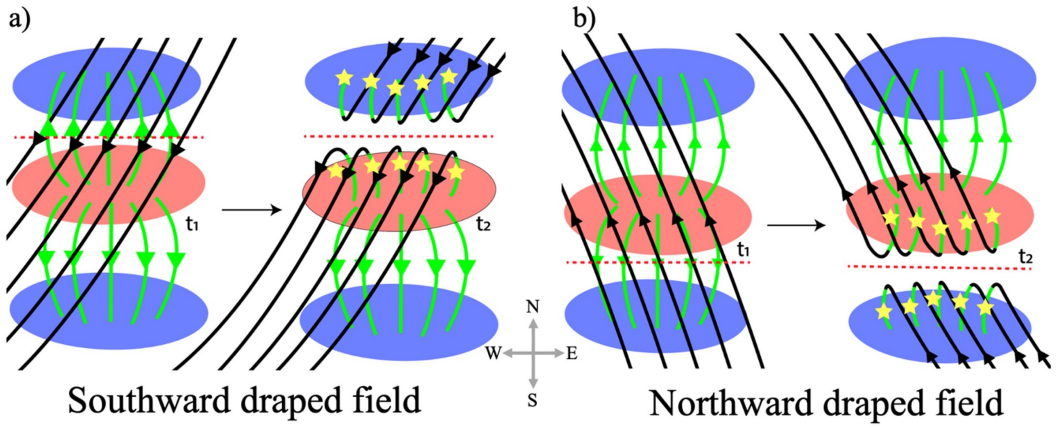


Figure 3. Schematic of draped field conditions that would result in magnetic reconnection with the (a) northward/ (b) southward anomalies within R_f. The black arrows represent the draped field, and the red dashed line represents the magnetic reconnection X-Line. The yellow stars represent the auroral emissions over the footprints.

ern mini-magnetosphere, causing discrete auroral emissions detectable by IUVS. The converse is true for a northward oriented draped IMF scenario. Under these conditions, the northward draped field is anti-parallel to and, therefore, more susceptible to reconnecting with the southern mini-magnetosphere. This would lead to the generation of open field lines and ultimately discrete auroral emissions over the footprints of the southern mini-magnetosphere (Figure 3b).

To test this hypothesis and understand the impact of draped IMF orientation on discrete auroral formation in the strong crustal field region at Mars, we set out to estimate the draped IMF orientation around R_f during the discrete auroral emission detections. First, we define an "interaction region" around Mars that estimates the general volume in which the draped field encounters the two mini-magnetospheres defined above. This interaction occurs at altitudes above the crustal magnetic fields (700 km < altitude) and in the lower southern hemisphere (latitude < –20° S). The 700 km altitude limit was chosen because it lies slightly above the estimated average altitude of the boundary between ionospheric plasma and shocked solar wind plasma at Mars (∼ 630 km, Holmberg et al. (2019)).

The crustal magnetic fields rotate with the planet and therefore vary in LT with the Martian day. Discrete auroral emission observations within R_f have been detected when this region was located at a variety of LTs, favoring the nightside/terminator regions both within the duskside sector (1800 < LT < 2400) and dawnside sector (0000 < LT < 0600) (e.g., Schneider et al., 2021; Johnston et al., 2023), shown in Figure 4. Nadir image scans were taken across all local times, suggesting the distribution shown in Figure 4 is not due to sampling bias. Therefore, we are interested in the draped field orientation in the LT sector in which R_f was positioned at the time of the discrete auroral emission. Duskside discrete auroral emissions are defined as events when R_f was located within 1800-2400 LT, and dawnside emissions are defined as events when R_f was located within 0000-0600 LT. All 49 discrete auroral emission events were detected along orbits that also sampled the associated interaction region.

To compare the draped field orientation to the crustal magnetic field geometry within R_f, we define a local clock angle measurement $\psi = arctan(B_E/B_N)$ where

This article is protected by copyright. All rights reserved.

Author Manuscript

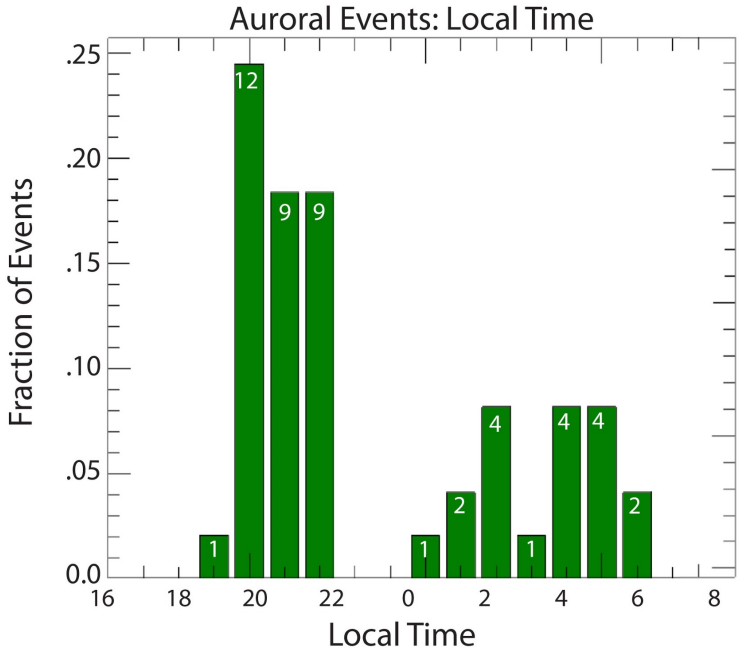


Figure 4. Histogram of local time in which R_f was positioned during discrete aurora emissions.

B_E, B_N are the eastward and northward components of the draped magnetic field in the planetary coordinate system. The crustal magnetic anomalies within R_f close northward and southward, so we are primarily interested in the north/south component of the draped magnetic field when assessing their susceptibility to undergo reconnection. Therefore, we calculate $|\psi|$, which distinguishes between northward ($0 \leq |\psi| \leq 90°$) and southward ($90 < |\psi| \leq 180°$) draped fields with east/west fields corresponding to the same value ($|\psi| = 90°$). We then average $|\psi|$ within the interaction region to estimate the draped field orientation on the duskside of the planet during the discrete auroral detection period.

3 Results

3.1 Case Study

An example of a discrete aurora event occurring within R_f on the duskside is displayed in Figure 5. IUVS detected an auroral emission at 06:18 UT on October 2, 2019, indicated by the green vertical line. The top two panels show the 3 component magnetic vector measurements taken by the MAG instrument in the MSO coordinate frame (Figure 5a) and the planetary coordinate system (Figure 5b). The blue vertical lines indicate the time range in which MAVEN sampled the associated interaction region for this event defined by the altitude (Figure 5d), latitude (Figure 5e), and LT (Figure 5f) of the spacecraft. This auroral emission was detected over R_f when R_f was positioned on the duskside sector at $\sim$ 2000 LT. The dominant component of the magnetic field within the interaction region is in the southward direction (Figure 5b), and our estimated draped field orientation within this region for this discrete aurora event is $|\psi|$=172°. The average altitude, latitude, and local time within this interaction region is 3252 km, −57.5°, and 16 LT, respectively. In

This article is protected by copyright. All rights reserved.

Author Manuscript

summary, we follow these steps to determine an associated draped field orientation over R_f during a discrete auroral emission:

1. Define the interaction region based on altitude (700 km < altitude), latitude (latitude < -20° S), and local time of the discrete auroral emission (either duskside (1800 < LT < 2400) or dawnside (0000 < LT < 0600).
2. Check if MAVEN sampled this region along the same orbit in which the discrete auroral emission was detected.
3. Calculate and average $|\psi| = |arctan(\frac{B_E}{B_N})|$ within the interaction region.

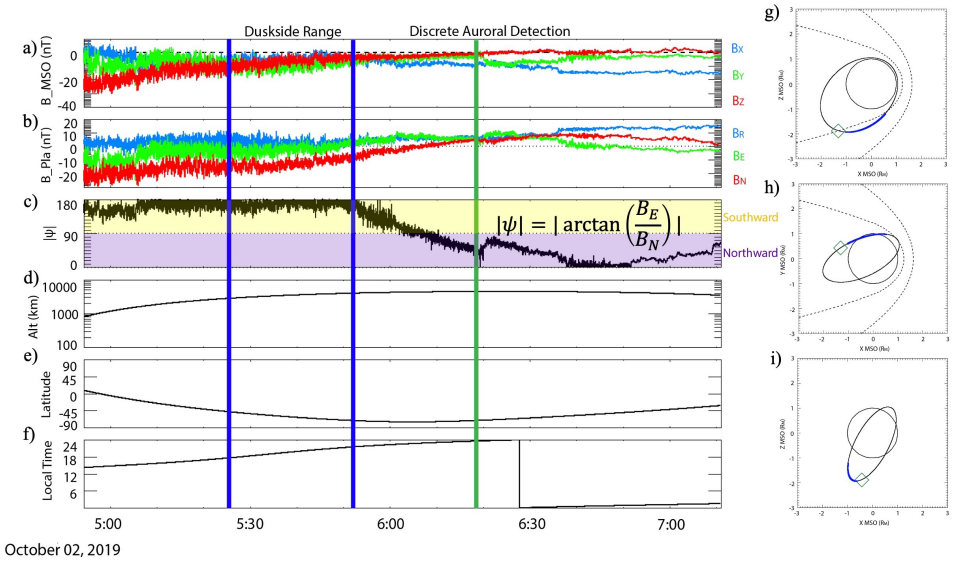


Figure 5. MAVEN observations on October 02, 2019 from 04:55-07:33 UT of the a) magnetic field in MSO frame (nT), b) magnetic field in planetary frame (nT), c) Absolute value of field local clock angle $|\psi|$ d) altitude of MAVEN e) Latitude of MAVEN f) Local time of MAVEN. The discrete auroral emission was detected when R_f was on the duskside of the planet, and the detection time is indicated by the green vertical line. The two blue vertical lines indicate the times in which MAVEN was sampling inside the interaction region associated with this discrete auroral event. MAVEN's orbital trajectory as viewed from the g) Z_{MSO} plane, h) Y_{MSO} plane, and i) X_{MSO} plane. The green diamond in panels (g)-(i) represent the location $MAVEN$ at the time of the discrete auroral detection. The blue segment along the orbit in panels (g)-(i) represent the range in which MAVEN sampled the interaction region associated with this discrete auroral event. The dashed lines in panels (g) and (h) show the nominal locations of the bowshock and magnetic pileup boundary from Trotignon et al. (2006).

3.2 Statistics

We repeat the analysis from Section 3.1 for all 49 of these events in which IUVS detected a discrete aurora event over R_f and MAVEN sampled the associated interaction region. To assess the orientation of the draped fields in relation to the crustal fields, orange and purple diamonds represent the location of the auroral emissions for southward ($|\psi| > 90°$) and northward ($|\psi| < 90°$) draped field conditions (Figure 6a). Of the 34 discrete auroral events that occur over the northern mini-magnetosphere, 29 (85%) are associated with southward draped fields. Of

This article is protected by copyright. All rights reserved.

Author Manuscript

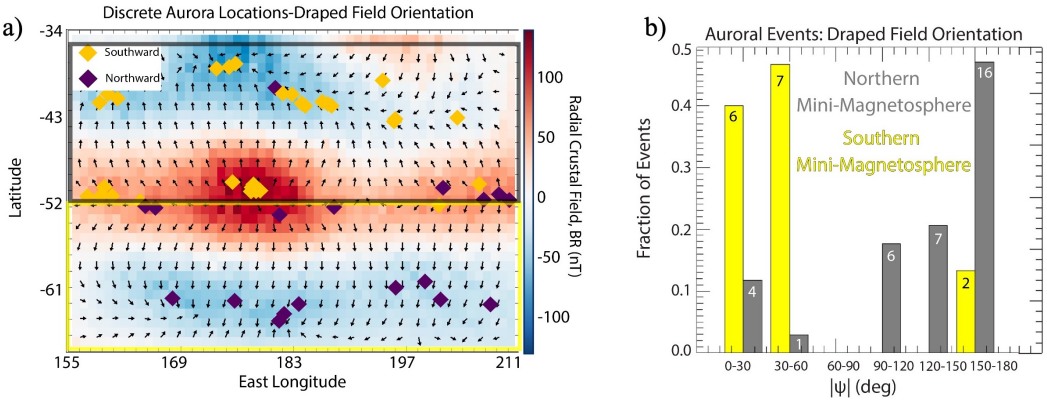


Figure 6. a) Map of data-derived crustal magnetic fields within R_f colored by the radial crustal field strength. The black arrows represent the transverse orientation of the crustal fields. Each diamond represents the spatial center of the 49 discrete auroral emission events detected by IUVS in which an associated draped field within the interaction region can be calculated. Orange diamonds represent events associated with southward draped fields and purple diamonds represent events associated with northward draped fields. b) Histogram of $|\psi|$ of the associated draped fields colored by the region in which the discrete auroral emission was detected.

the 15 discrete auroral events that occur over the southern mini-magnetosphere, 13 (87%) are associated with northward draped fields. The distribution of $|\psi|$ (Figure 6) demonstrates that discrete auroral events occurred more often for draped fields that point primarily southward and northward, rather than eastward/westward, supporting the hypothesis that anti-parallel reconnection likely played a role in the onset of these events.

The locations of discrete auroral emission over R_f also show a trend with LT, as reported in Johnston23. The discrete auroral emission location, represented as a diamond in Figure 7, is colored by the LT sector in which the detection location was positioned at the time of the spectrograph image taken by IUVS. Of the 34 events that occur over the footprints of the northern mini-magnetosphere, 29 (85%) are detected when R_f is on the duskside ($1800 < \text{LT} < 2400$). Of the 15 events that occur over the footprints of the southern anomaly, 13 (87%) are detected when R_f is on the dawnside ($0000 < \text{LT} < 0600$). We find an important correlation between the trends in LT and the draped field trend described above that we apply to the reconnection hypothesis: 97% of events with associated northward fields occur when R_f is on the dawnside and 94% of events with associated southward fields occur when R_f is on duskside.

Now that we have identified a connection between the LT and draped field preference for discrete aurora, we investigate the upstream magnetospheric conditions that favor discrete auroral emissions within R_f. We do this by plotting the fraction of events as a function of upstream IMF clock angle ($\theta = arctan(BY_{MSO}/BZ_{MSO})$) during the discrete auroral events. Here, BY_{MSO} and BZ_{MSO} represent the $\hat{Y}$ and $\hat{Z}$ component of the magnetic field in the MSO coordinate system. We note that θ is a measurement of the upstream IMF clock angle in MSO coordinates, while ψ is a locally defined clock angle measurements of the draped IMF in the planetary coordinate system. Of the 49 events within R_f, we were able to estimate the upstream IMF orientation for 44 events utilizing the methods of Halekas et al. (2017) and Ruhunusiri et al. (2018) as outlined in Section 2.1.

This article is protected by copyright. All rights reserved.

Author Manuscript

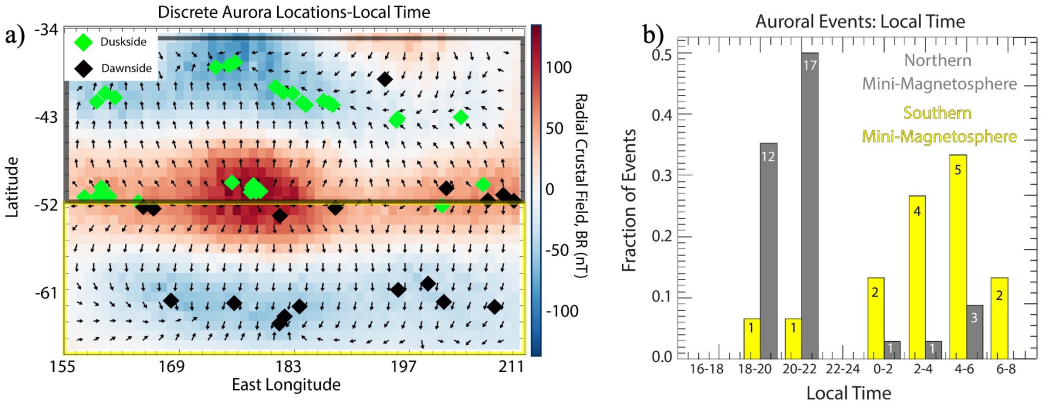


Figure 7. a) Same crustal field maps as Figure 6. Each diamond now represents the spatial center of all 49 discrete auroral emission events within R_f, with green diamonds representing events that occurred on the duskside ($1800 < \text{LT} < 2400$) of the planet and black diamonds representing events that occurred on the dawnside of the planet ($0000 < \text{LT} < 0600$). b) Histogram of the local time of the discrete auroral emission colored by the region in which the discrete auroral emission was detected. Adapted from Johnston23.

From these 44 events with upstream IMF information, 30 and 14 were associated with the northern and southern mini-magnetospheres, respectively. Figure 8a is similar to Figure 6a and 7a, but here each diamond is colored by the Y_{MSO} component of the IMF during each discrete auroral event, with blue diamonds representing IMF -BY_{MSO} ($\theta < 0°$) upstream conditions and pink diamonds representing IMF +BY_{MSO} ($\theta > 0°$) conditions. Of the 44 events with upstream IMF conditions

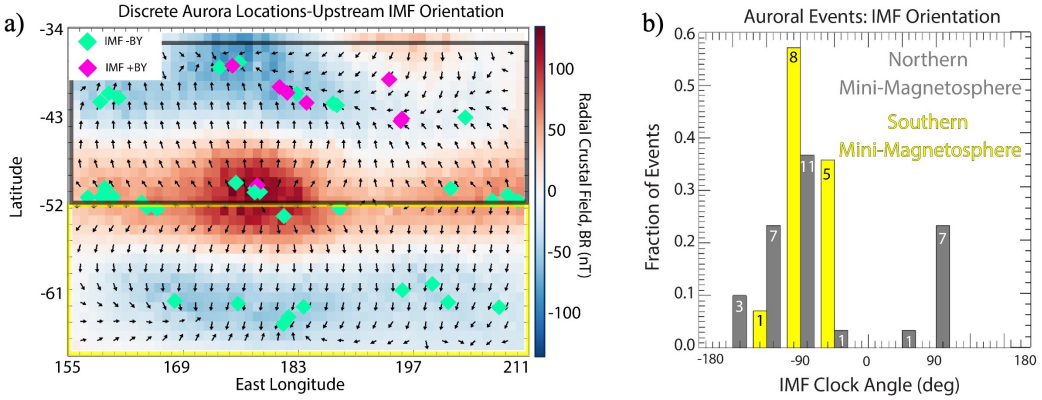


Figure 8. a) Same crustal field maps as Figure 6 and 7. Each diamond now represents the spatial center of the 44 discrete auroral emission events with upstream IMF information available with blue diamonds representing events with associated IMF -BY_{MSO} orientation ($\theta < 0°$) and pink diamonds representing events with associated IMF +BY_{MSO} orientation ($\theta > 0°$). b) Histogram of estimated upstream IMF clock angle during each discrete aurora event, colored by the region in which the discrete aurora emission was detected.

available, 36 (82%) are associated with IMF -BY_{MSO} conditions. Of the 30 (14)

This article is protected by copyright. All rights reserved.

Author Manuscript

events that occurred over the northern (southern) mini-magnetosphere, 22 (73%) [14 (100%)] occur under IMF -BY_{MSO} conditions. 8 of the events were associated with IMF +BY_{MSO} conditions. The preference for IMF -BY_{MSO} conditions is further demonstrated in the histogram of Figure 8b where the majority of the discrete auroral events occur when -180° < θ < 0°.

3.3 Nominal Draped Magnetic Field Conditions

To further investigate the trends with magnetospheric conditions and discrete auroral emission, we perform a statistical analysis of the shocked IMF orientation at Mars. A statistical survey of draped IMF orientations will better our understanding of the connections between the draped field orientation, LT, and upstream IMF clock angle conditions that generate discrete aurora. To do so, we assess MAG measurements within the shocked solar wind from November 1, 2014 through December 30, 2020, regardless of whether or not discrete aurora were detected. We select for orbits in which apoapsis was on the nightside of the planet and R_f was positioned on the terminator/nightside of Mars. We divide the Martian magnetosphere into the duskside ($Y_{MSO} > 0$) and dawnside ($Y_{MSO} < 0$) perspectives and spatially bin the data in the XZ_{MSO} plane into $0.2R_M \times 0.2R_M$ bins where R_M is the radius of

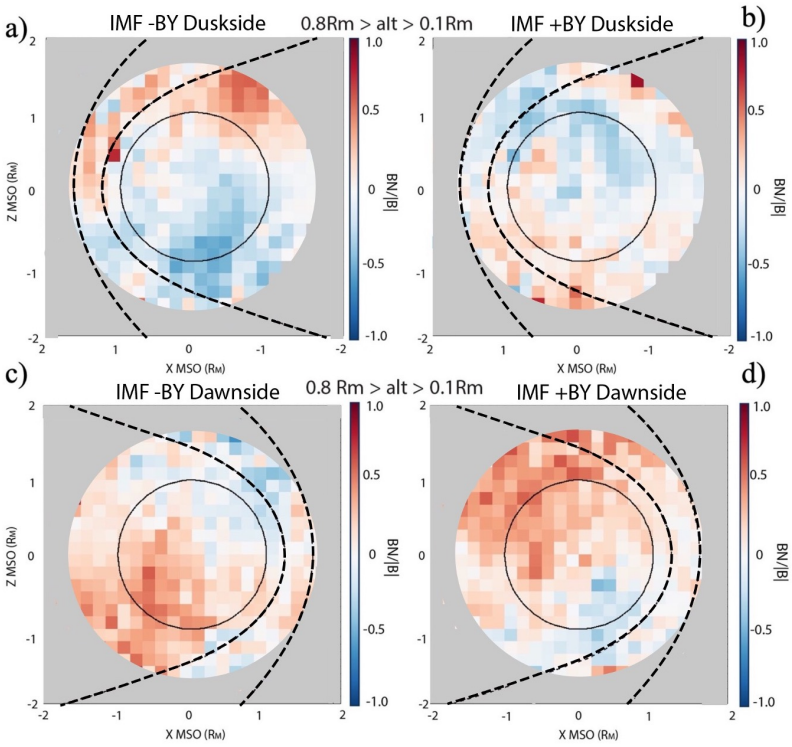


Figure 9. Magnetic map of the averaged $B_N/|B|$ value taken from MAVEN MAG measurements at altitudes from 0.1 R_M to 0.8 R_M from November 1, 2014 through December 30, 2020 of the XZ_{MSO} plane. (a), (b) are maps for magnetic fields on the duskside of Mars (1200 < LT < 2400) for IMF $\mp$ BY conditions. (c), (d) are maps for magnetic fields on the dawnside ((0000 < LT < 2400)) for IMF $\mp$ BY conditions. The bins are colored by the averaged $B_N/|B|$ with red indicating northward fields and blue indicating southward fields. The dashed lines in panels show the nominal locations of the bowshock and magnetic pileup boundary from (Trotignon et al., 2006).

This article is protected by copyright. All rights reserved.

Author Manuscript

Mars (3389.5 km). From 7200 orbits, we measure the average magnetic field orientation within each spatial bin in the altitude range of $0.1R_M$ – $0.8R_M$ on both the dawnside and duskside of the planet. Thus, for both the dawnside and duskside of the planet, we measure the average magnetic field within half of a spherical shell with radius from $0.1R_M$ – $0.8R_M$. We then project this average magnetic field onto the XZ_{MSO} plane in Figure 9.

For our purposes, we are most interested in the northward/southward component of the draped magnetic field, so we average the value of $B_N/|B|$ within each bin, where B_N is the $\hat{N}$ component of the magnetic field in planetary coordinates. We then separate the magnetic field measurements based on the upstream IMF BY_{MSO} component. The IMF orientation was again estimated via combination of in situ solar wind measurements (Halekas et al., 2017) and magnetosheath proxy values (Ruhunusiri et al., 2018) for IMF when direct measurements are not available, as described above in Section 2.1.

The nominal draped field orientation as viewed from the duskside and dawnside of the planet under different upstream IMF BY_{MSO} conditions is shown in Figure 9.These magnetic maps provide insight into the global draping pattern of the IMF around Mars. On the duskside, the draped IMF is predominately southward (blue) on the nightside($-1.8R_M < X_{MSO} < 0$) of Mars, under IMF $-BY_{MSO}$ conditions (Figure 9a). On the duskside under $+BY_{MSO}$ conditions, the magnetic field points primarily east/west (white), with a slight overall preference to point southwards on the nightside (Figure 9b). The opposite is true on the dawnside, where there is a prevalence of northward-directed draped IMF (red) on the nightside of Mars for both IMF $\mp BY_{MSO}$ conditions (Figure 9c, 9d).

4 Discussion

4.1 Trends in Discrete Aurora Formation

Based on our analysis of MAVEN MAG data available during discrete auroral events at Mars, we have revealed three magnetospheric trends related to discrete auroral formation over the two mini-magnetospheres that comprise the R_f region:

1. Discrete auroral emissions occurring within the northern (southern) mini-magnetosphere are associated with southward-directed (northward-directed) draped magnetic field conditions (Figure 6).
2. When R_f is positioned on the duskside (dawnside) sector, discrete aurora predominately occur in the northern (southern) mini-magnetosphere (Figure 7).
3. For a majority of the time, discrete auroral emissions over both the northern and southern mini-magnetospheres within R_f occur when the upstream IMF is pointed in the -Y_{MSO} direction (Figure 8).

Result (1) supports the hypothesis that magnetic reconnection between the crustal anomalies and the draped magnetic fields plays a role in discrete auroral formation over the two mini-magnetospheres within R_f. Of the 49 discrete auroral events with measurable associated draped field conditions, 42 (86%) occur when the draped magnetic field orientation is anti-parallel to and therefore, susceptible to reconnection with, the underlying crustal anomaly (Figure 3). We note that of the 7 events that occur under draped field conditions that are not susceptible to reconnection with the underlying crustal anomaly, 6 occur within the radially outward region within R_f, near the border between the northern and southern mini-magnetosphere. This radially outward region is magnetically connected to both the northern mini-magnetosphere and the southern mini-magnetosphere. As a result, it is possible that

This article is protected by copyright. All rights reserved.

Author Manuscript

some of the events within this radially outward region were misclassified regarding which mini-magnetosphere they were associated with. Therefore, there may only be one event ($\sim$ -40°Lat, 180°Lon) that does not support the reconnection hypothesis.

Magnetic reconnection between these mini-magnetospheres and the draped IMF generates open magnetic field lines which connect the lower ionosphere directly to high energy solar wind plasma. These open field lines additionally create electric potential structures that accelerate magnetospheric electrons into the auroral electron energy range (Poppe et al., 2021). We therefore posit that magnetic reconnection is a necessary precursor to the discrete aurora phenomenon.

Result (1) is the first to relate magnetic reconnection to discrete aurora, thereby enhancing our understanding of the local magnetospheric conditions that lead to the onset of discrete auroral emissions at Mars (i.e., anti-parallel magnetic field regimes). This result may inform our understanding of the location of discrete auroral emissions under certain local magnetospheric conditions with respect to the underlying crustal magnetic field geometry, both within and outside of R_f. Models of discrete aurora formation under a variety of magnetospheric conditions can extrapolate from result (1) to better model the location and frequency of discrete aurora formation at Mars.

Results (2) and (3) have been previously reported in other discrete auroral data sets (Schneider et al., 2021) and are also present in precipitating electron measurements within R_f (Xu et al., 2022). When viewed through the lens of the reconnection hypothesis, the draped field pattern shown in Figure 9 helps explain results (2) and (3). R_f is in the southern hemisphere, and discrete auroral emissions occur most frequently within the nightside-terminator region (Figure 4). Therefore, we are most interested in the draped field orientation surrounding the southern/nightside-terminator of the planet. Magnetic reconnection involving the northern mini-magnetosphere would favor southward draped magnetic fields, which are most prevalent in the southern/nightside-terminator region on the duskside of the planet under IMF -BY_{MSO} conditions (Figure 9a). When we consider the southern mini-magnetosphere, magnetic reconnection would now favor northward draped magnetic fields, which are most prevalent in the southern/nightside-terminator region on the dawnside of the planet under IMF -BY_{MSO} conditions (Figure 9c). These are the exact trends we see in both discrete auroral observations and auroral electrons (Xu et al., 2022) around the two crustal mini-magnetospheres that comprise R_f [results (2) and (3)].

We note that recent studies have demonstrated open magnetic topology measurements on the nightside of Mars respond to changes in the $\pm$ Y_{MSO} component of the IMF (e.g., Brain et al., 2020; Weber et al., 2020). These studies also revealed a trend in open magnetic topology measurements with respect to local time on the nightside. These studies viewed open topology rates globally and found that under fixed upstream IMF conditions, crustal magnetic field regimes that tend to be open on the duskside, tend to be closed on the dawnside, and vice versa. Discrete aurora are associated with open magnetic fields, and, therefore, our study supports this result by highlighting connection between discrete aurora, local time, and magnetic reconnection within R_f.

4.2 Discrete Aurora and IMF Draping

The draping pattern shown in Figure 9 helps demonstrate the onset of discrete auroral from a more global perspective. It has been suggested that the draping pattern within the altitude range depicted in Figure 9 is itself a result of the convectional electric field ($\mathbf{E}$ = -$\mathbf{v}_{sw}$ $\times$ $\mathbf{B}_{IMF}$) (e.g., Dubinin et al., 2019; Chai et al., 2019; Zhang et al., 2022). On the dayside of the planet, planetary ions are accelerated into

This article is protected by copyright. All rights reserved.

Author Manuscript

the +E hemisphere, creating the ion plume (Dong et al., 2015). Due to the conservation of momentum, the ion plume on the dayside will accelerate solar wind ions into the -E hemisphere on the nightside, creating the "ion trail" (Dubinin et al., 2019). The frozen-in field condition causes the magnetic field around the planet to move with the flowing plasma, which generates a tilted draped field. The direction of this tilt is controlled by the orientation of **E**, which is largely determined by the clock angle of the IMF because $\mathbf{v}_{sw}$ is generally moving in the anti-sunward ($-X_{MSO}$) direction.

Figure 10 illustrates this draping pattern, with the crustal anomalies within

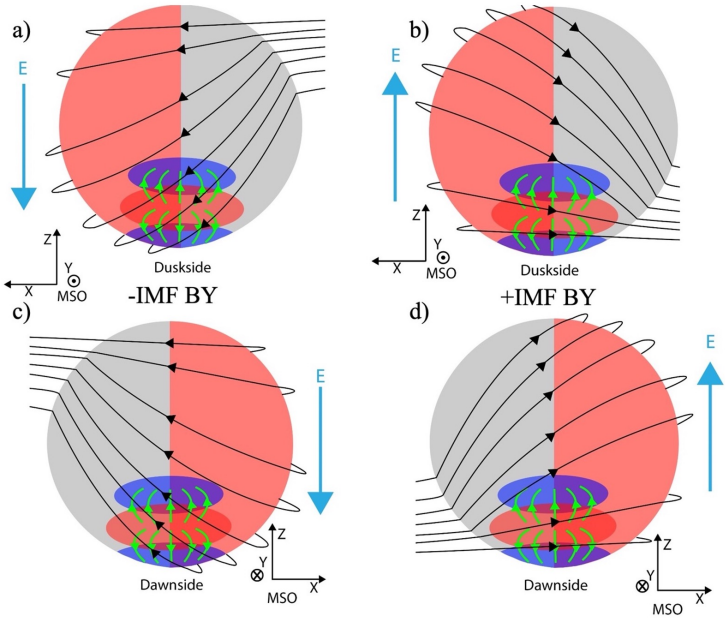


Figure 10. Schematics of the draped magnetic field configuration around Mars under different convectional electric field conditions. (a), (b) are views of the magnetic field draping on the duskside of Mars ($Y_{MSO} > 0$) for IMF $\mp BY$ conditions. (c), (d) are schematics of the magnetic field orientations on the dawnside ($Y_{MSO} < 0$) for IMF $\mp BY$ conditions. Mars is divided into the dayside (pink) and nightside (grey) hemispheres. The light blue arrow represents the direction of the convectional electric field. The black arrows represent the direction of the draped magnetic field. The blue/red ovals represent the radially inward/outward crustal magnetic fields regions, and the green arrows represent the transverse component of the two crustal anomalies within R_f. The crustal anomalies have been enlarged for clarity.

R_f projected onto the terminator of the planet and enlarged for clarity. Under IMF -BY_{MSO} conditions, **E** points towards the southern hemisphere. This tilts the draped magnetic fields and creates more southward (northward) draped fields in the southern hemisphere on the duskside (dawnside) of the planet, which is seen in the data-derived magnetic field maps (Figures 9a, 9c). This tilt helps explain why there is an IMF -BY_{MSO} preference for discrete aurora emissions over R_f. For the IMF -BY_{MSO} case, **E** points towards the southern hemisphere and the draped field presents more north/south magnetic field orientations in the nightside-terminator region of the southern hemisphere compared to the IMF +BY_{MSO} case. For the IMF +BY_{MSO} case, **E** points toward the northern hemisphere and the tilted draped

This article is protected by copyright. All rights reserved.

Author Manuscript

magnetic fields point more southward (northward) in the northern hemisphere on the duskside (dawnside).

Figure 9 and Figure 10 illustrate that the IMF -BY_{MSO} scenario presents more northward/southward draped fields to the strong crustal fields within R_f compared to the IMF +BY_{MSO} scenario because of the larger degree of tilted draped fields in the +E hemisphere. These northward/southward draped fields over R_f would be more anti-parallel to the underlying crustal anomalies within R_f, and would, as a result, favor magnetic reconnection. We note, however, that the data presented in Figure 9 is a subset of the data set used to construct the E-field induced draped magnetic field patterns described in Chai et al. (2019) and Zhang et al. (2022) and illustrated in Figure 10. The $0.1R_M - 0.8R_M$ altitude restriction for the MAG measurements presented in Figure 9 captures the E-field controlled tilt in IMF draping, but also likely captures other draped field effects not discussed here. These effects include circumpolar draped fields (Zhang et al., 2022), looped magnetic fields (Chai et al., 2019), and draped field tilt in response to solar wind plasma diversion around the planet (e.g., Fang et al., 2018; Dong et al., 2019).

The convectional electric field strongly influences the magnetic field draping patterns and produces results (1)-(3) described above (Figure 11). Figure 11a high-

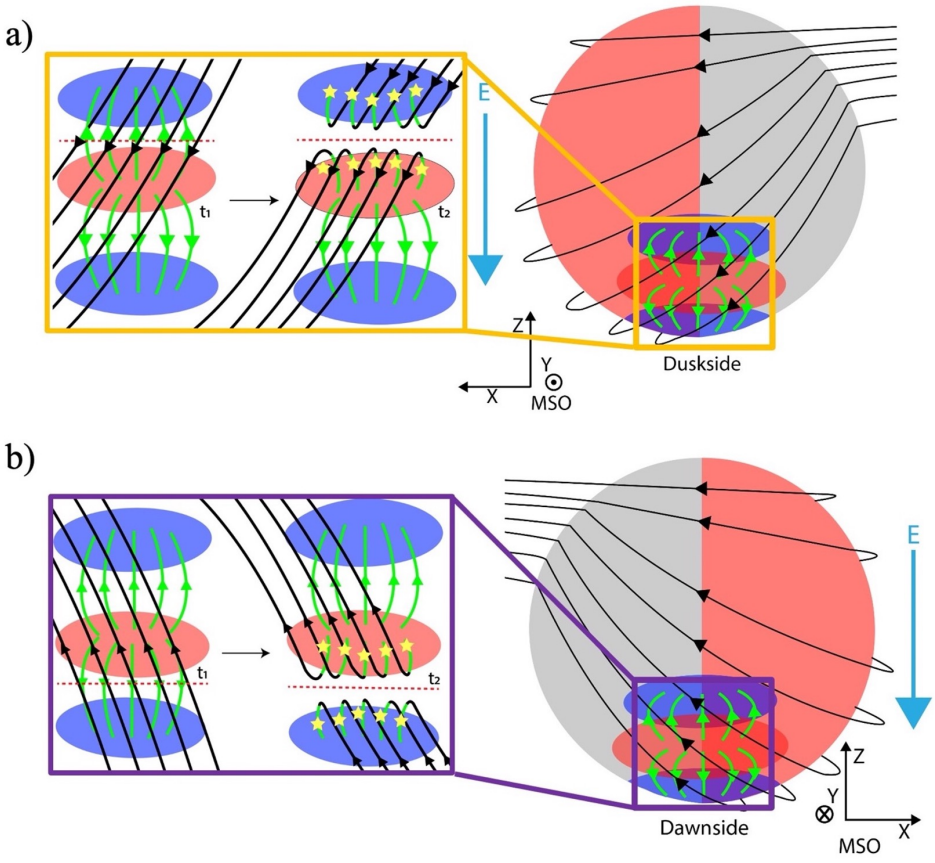


Figure 11. Combined schematics taken from Figures 1 and Figures 8a,c. Shows the draped magnetic field (black arrows) draping around Mars under IMF -BY_{MSO} conditions as seen from the duskside (a) and dawnside (b). The panels to the right show a zoomed in schematic of the draped field reconnecting with the northern anomaly (a) and the southern anomaly (b) and producing discrete auroral emissions (yellow stars).

This article is protected by copyright. All rights reserved.

Author Manuscript

lights the case for discrete aurora activation over the footprints of the northern mini-magnetosphere. The northern mini-magnetosphere closes northward and is therefore more susceptible to magnetic reconnection with southward draped magnetic fields (result (1), Figure 6). Over R_f, the draped magnetic field points southward on the duskside (result (2), Figure 7) and under IMF -BY_{MSO} conditions (result (3), Figure 8). Figure 11b highlights the case for discrete auroral emission over the footprints of the southern mini-magnetosphere. The southern mini-magnetosphere closes southward and is more susceptible to magnetic reconnection with northward draped magnetic fields (result (1), Figure 6). Over R_f, the draped magnetic field points northward on the dawnside (result (2), Figure 7) and under IMF -BY_{MSO} conditions (result (3), Figure 8). Therefore, our results suggest that this draping process of the IMF fields around Mars determines the magnetic field configuration on the terminators, and, within R_f, this configuration favors magnetic reconnection with the northern mini-magnetosphere on the duskside and the southern mini-magnetosphere on the dawnside for an upstream IMF oriented in the -Y_{MSO} direction. Therefore, results (1)-(3) lay a framework for understanding discrete auroral formation from a global point of view.

Our study strongly supports the hypothesis that magnetic reconnection is a precursor to discrete aurora over R_f. Magnetic reconnection changes magnetic topology and "opens-up" the crustal anomalies to the solar wind particles. These open fields allow for direct access to high-energy solar wind electrons and also generate potential structures that accelerate ionospheric electrons. These high-energy electrons eventually deposit their energy into the atmosphere, generating discrete aurora. However, questions remain regarding the timescales of the processes that influence the onset of discrete aurora at Mars. How quickly after the onset of magnetic reconnection is auroral light emitted? Discrete auroral emissions tend to occur near the terminator on the nightside ($19 < \text{LT} < 21$ and $2 < \text{LT} < 5$, Figure 4). Figures 9a and 9c demonstrate that the ideal draped field conditions for magnetic reconnection over R_f occur when $-1 < X_{MS0} < 0$, which also corresponds to the nightside-terminator region on the surface of the planet. This suggests that discrete auroral emissions occurred near magnetospheric regions that were ideal for magnetic reconnection, implying the timescale for the chain of events that resulted in discrete aurora did not exceed the time for the planet to rotate significantly into different local time regimes ($\sim$ 3 hours).

Furthermore, Figure 1 shows discrete auroral observations occur across the nightside of Mars, not only within R_f. It is possible that magnetic reconnection also plays a role in the emission of discrete aurora around mini-magnetospheres sourced by other crustal anomalies, or perhaps different magnetospheric processes take place to produce the auroral electrons that cause discrete aurora away from R_f. We note that the trends in LT and upstream IMF for discrete aurora over R_f do not hold for discrete auroral emissions outside of R_f. Future studies should investigate discrete auroral observations over other crustal anomaly regions on Mars outside of R_f to elucidate if any analogous trends with draped magnetic field orientation are present over these regions. Also, the new Emirates Mars Mission (EMM) spacecraft has shed new light onto discrete aurora at Mars. While EMM does not have a magnetometer instrument onboard, the Emirates Mars Ultraviolet Spectrometer (EMUS) instrument (Holsclaw et al., 2021) is very sensitive to far UV auroral emissions and has detected a variety of interesting auroral phenomena at Mars (e.g., R. J. Lillis et al., 2022; Chaffin et al., 2022). A future collaborative study utilizing the imaging capacity of EMUS with magnetic field measurements by MAVEN will help further our understanding of the mini-magnetospheric processes that control the onset of discrete aurora at Mars.

This article is protected by copyright. All rights reserved.

Author Manuscript

5 Conclusions

Here, we present an analysis to explore the hypothesis that magnetic reconnection between the underlying crustal magnetic fields and the draped IMF plays a role in the onset of discrete aurora over the footprints of two crustal anomalies. We analyze 49 discrete auroral detections observed via nadir scans of Mars by the IUVS instrument onboard MAVEN over R_f. Using the MAG instrument onboard MAVEN, we find that discrete auroral events that occur over the footprints of the northern mini-magnetosphere are associated with southward draped fields over R_f, and those that occur over the footprints of the southern mini-magnetosphere are associated with northward draped fields over R_f. This trend supports the hypothesis that anti-parallel magnetic reconnection plays a role in discrete auroral formation over this region of crustal magnetism. We further investigate trends in local time and upstream IMF conditions by creating magnetic maps of the draped field around Mars under different IMF conditions. We demonstrate that in the southern hemisphere, an IMF directed in the -Y_{MSO} orientation begins to shift southward on the duskside as it drapes around Mars and presents anti-parallel magnetic field lines to northern mini-magnetosphere, which would result in reconnection and discrete aurora over the footprints of the northern mini-magnetosphere. The opposite is true on the dawnside, where the IMF is shifted northward in the southern hemisphere and reconnects with the southern mini-magnetosphere, resulting in discrete aurora emissions over the footprints of the southern mini-magnetosphere. The reconnection hypothesis explored in this study helps answer questions regarding previously unexplained trends in local time and upstream IMF conditions for discrete auroral emissions and lays out a framework for understanding the discrete auroral phenomena at Mars from a mini-magnetospheric perspective.

Data Availability

In accordance with the AGU data policy, MAVEN data are publicly available through the Planetary Plasma Interactions Node of the Planetary Data System (https://pds-ppi.igpp.ucla.edu/mission/MAVEN).

Acknowledgments

The MAVEN project is supported by NASA through the Mars Exploration Program. We acknowledge support from the Future Investigators in NASA Earth and Space Science and Technology research grant (award number 80NSSC21K1530) for C. Bowers' graduate student research. N.R. is supported by NASA under award number 80GSFC21M0002.

References

Acuña, M. H., Connerney, J. E., Ness, N. F., Lin, R. P., Mitchell, D., Carlson, C. W., ... Cloutier, P. (1999). Global distribution of crustal magnetization discovered by the mars global surveyor mag/er experiment [Journal Article]. *Science*, *284*(5415), 790-3. Retrieved from `https://www.ncbi.nlm.nih.gov/pubmed/10221908` doi: 10.1126/science.284.5415.790

Angelopoulos, V., McFadden, J. P., Larson, D., Carlson, C. W., Mende, S. B., Frey, H., ... Kepko, L. (2008). Tail reconnection triggering substorm onset. *Science*, *321*(5891), 931-935. Retrieved from `https://www.science.org/doi/abs/10.1126/science.1160495` doi: 10.1126/science.1160495

Bertaux, J., Leblanc, F., Witasse, O., Quemerais, E., Lilensten, J., Stern, S., ... Korablev, O. (2005). Discovery of an aurora on mars [Journal Article]. *Nature*, *435*(7043), 790-794. doi: 10.1038/nature03603

This article is protected by copyright. All rights reserved.

Author Manuscript

Bowers, C. F., Slavin, J. A., DiBraccio, G. A., Poh, G., Hara, T., Xu, S., & Brain, D. (2021). Maven survey of magnetic flux rope properties in the martian ionosphere: Comparison with three types of formation mechanisms. *Geophysical Research Letters*, *48*(10), e2021GL093296. Retrieved from https://agupubs.onlinelibrary.wiley.com/doi/abs/10.1029/2021GL093296 doi: https://doi.org/10.1029/2021GL093296

Brain, D., Baker, A., Briggs, J., Eastwood, J., Halekas, J., & Phan, T. (2010). Episodic detachment of martian crustal magnetic fields leading to bulk atmospheric plasma escape [Journal Article]. *Geophysical Research Letters*, *37*. doi: 10.1029/2010GL043916

Brain, D., & Halekas, J. S. (2012). Aurora in martian mini magnetospheres. In *Auroral phenomenology and magnetospheric processes: Earth and other planets* (p. 123-132). American Geophysical Union (AGU). Retrieved from https://agupubs.onlinelibrary.wiley.com/doi/abs/10.1029/2011GM001201 doi: https://doi.org/10.1029/2011GM001201

Brain, D., Halekas, J. S., Peticolas, L. M., Lin, R. P., Luhmann, J. G., Mitchell, D. L., ... Rme, H. (2006). On the origin of aurorae on mars. *Geophysical Research Letters*, *33*(1). Retrieved from https://agupubs.onlinelibrary.wiley.com/doi/abs/10.1029/2005GL024782 doi: https://doi.org/10.1029/2005GL024782

Brain, D., Lillis, R., Mitchell, D., Halekas, J., & Lin, R. (2007). Electron pitch angle distributions as indicators of magnetic field topology near mars [Journal Article]. *Journal of Geophysical Research-Space Physics*, *112*(A9). doi: 10.1029/2007JA012435

Brain, D., Weber, T., Xu, S., Mitchell, D., Lillis, R., Halekas, J., ... Jakosky, B. (2020). Variations in nightside magnetic field topology at mars [Journal Article]. *Geophysical Research Letters*, *47*(19). doi: 10.1029/2020GL088921

Chaffin, M. S., Fowler, C. M., Deighan, J., Jain, S., Holsclaw, G., Hughes, A., ... AlMatroushi, H. (2022). Patchy proton aurora at mars: A global view of solar wind precipitation across the martian dayside from emm/emus. *Geophysical Research Letters*, *49*(17), e2022GL099881. Retrieved from https://agupubs.onlinelibrary.wiley.com/doi/abs/10.1029/2022GL099881 doi: https://doi.org/10.1029/2022GL099881

Chai, L., Wan, W., Wei, Y., Zhang, T., Exner, W., Fraenz, M., ... Zhong, J. (2019). The induced global looping magnetic field on mars [Journal Article]. *Astrophysical Journal Letters*, *871*(2). doi: 10.3847/2041-8213/aaff6e

Cloutier, P., Law, C., Crider, D., Walker, P., Chen, Y., Acuna, M., ... Ness, N. (1999). Venus-like interaction of the solar wind with mars [Journal Article]. *Geophysical Research Letters*, *26*(17), 2685-2688. doi: 10.1029/1999GL900591

Connerney, J., Espley, J., Lawton, P., Murphy, S., Odom, J., Oliversen, R., & Sheppard, D. (2015). The maven magnetic field investigation [Journal Article]. *Space Science Reviews*, *195*(1-4), 257-291. doi: 10.1007/s11214-015-0169-4

Cravens, T., Fowler, C., Brain, A., D.A.and Rahmati, Xu, S., Ledvina, S., Andersson, L., & Renzaglia, A. (2020). Magnetic reconnection in the ionosphere of mars: The role of collisions [Journal Article]. *Journal of Geophysical Research-Space Physics*, *125*(9). doi: 10.1029/2020JA028036

Deighan, J., Jain, S., Chaffin, M., Fang, X., Halekas, J., Clarke, J., ... Jakosky, B. (2018). Discovery of a proton aurora at mars [Journal Article]. *Nature Astronomy*, *2*(10), 802-807. doi: 10.1038/s41550-018-0538-5

Dong, Y., Fang, X., Brain, D., McFadden, J. P., Halekas, J. S., Connerney, J. E., ... Jakosky, B. M. (2015). Strong plume fluxes at mars observed by maven: An important planetary ion escape channel. *Geophysical Research Letters*, *42*(21), 8942-8950. Retrieved from https://agupubs.onlinelibrary.wiley.com/doi/abs/10.1002/2015GL065346 doi: https://doi.org/10.1002/2015GL065346

This article is protected by copyright. All rights reserved.

Author Manuscript

Dong, Y., Fang, X., Brain, D. A., Hurley, D. M., Halekas, J. S., Espley, J. R., ... Jakosky, B. M. (2019). Magnetic field in the martian magnetosheath and the application as an imf clock angle proxy. *Journal of Geophysical Research: Space Physics*, *124*(6), 4295-4313. Retrieved from https://agupubs.onlinelibrary.wiley.com/doi/abs/10.1029/2019JA026522 doi: https://doi.org/10.1029/2019JA026522

Dubinin, E., Modolo, R., Fraenz, M., Paetzold, M., Woch, J., Chai, L., ... Zelenyi, L. (2019). The induced magnetosphere of mars: Asymmetrical topology of the magnetic field lines [Journal Article]. *Geophysical Research Letters*, *46*(22), 12722-12730. doi: 10.1029/2019GL084387

Dubinin, E., Modolo, R., Fraenz, M., Woch, J., Duru, F., Akalin, F., ... Picardi, G. (2008). Structure and dynamics of the solar wind/ionosphere interface on mars: Mex-aspera-3 and mex-marsis observations. *Geophysical Research Letters*, *35*(11). Retrieved from https://agupubs.onlinelibrary.wiley.com/doi/abs/10.1029/2008GL033730 doi: https://doi.org/10.1029/2008GL033730

Eastwood, J. P., Brain, D. A., Halekas, J. S., Drake, J. F., Phan, T. D., ieroset, M., ... Acua, M. (2008). Evidence for collisionless magnetic reconnection at mars. *Geophysical Research Letters*, *35*(2). Retrieved from https://agupubs.onlinelibrary.wiley.com/doi/abs/10.1029/2007GL032289 doi: https://doi.org/10.1029/2007GL032289

Ebert, R. W., Fuselier, S. A., Allegrini, F., Bagenal, F., Bolton, S. J., Clark, G., ... Wilson, R. J. (2022). Evidence for magnetic reconnection at ganymede's upstream magnetopause during the pj34 juno flyby. *Geophysical Research Letters*, *49*(23), e2022GL099775. Retrieved from https://agupubs.onlinelibrary.wiley.com/doi/abs/10.1029/2022GL099775 (e2022GL099775 2022GL099775) doi: https://doi.org/10.1029/2022GL099775

Fang, X., Ma, Y., Luhmann, J., Dong, Y., Brain, D., D.A.and Hurley, Dong, C., ... Jakosky, B. (2018). The morphology of the solar wind magnetic field draping on the dayside of mars and its variability [Journal Article]. *Geophysical Research Letters*, *45*(8), 3356-3365. doi: 10.1002/2018GL077230

Fang, X., Ma, Y., Schneider, N., Girazian, Z., Luhmann, J., Milby, Z., ... Jakosky, B. (2022). Discrete aurora on the nightside of mars: Occurrence location and probability. *Journal of Geophysical Research: Space Physics*, *127*(3), e2021JA029716. Retrieved from https://agupubs.onlinelibrary.wiley.com/doi/abs/10.1029/2021JA029716 doi: https://doi.org/10.1029/2021JA029716

Fowler, C. M., Agapitov, O. V., Xu, S., Mitchell, D. L., Andersson, L., Artemyev, A., ... Mazelle, C. (2020). Localized heating of the martian topside ionosphere through the combined effects of magnetic pumping by large-scale magnetosonic waves and pitch angle diffusion by whistler waves. *Geophysical Research Letters*, *47*(5), e2019GL086408. Retrieved from https://agupubs.onlinelibrary.wiley.com/doi/abs/10.1029/2019GL086408 doi: https://doi.org/10.1029/2019GL086408

Fowler, C. M., Hanley, K. G., McFadden, J. P., Chaston, C. C., Bonnell, J. W., Halekas, J. S., ... Lillis, R. J. (2021). Maven observations of low frequency steepened magnetosonic waves and associated heating of the martian nightside ionosphere. *Journal of Geophysical Research: Space Physics*, *126*(10), e2021JA029615. Retrieved from https://agupubs.onlinelibrary.wiley.com/doi/abs/10.1029/2021JA029615 doi: https://doi.org/10.1029/2021JA029615

Frey, H. U. (2007). Localized aurora beyond the auroral oval. *Reviews of Geophysics*, *45*(1). Retrieved from https://agupubs.onlinelibrary.wiley.com/doi/abs/10.1029/2005RG000174 doi: https://doi.org/10.1029/2005RG000174

This article is protected by copyright. All rights reserved.

Author Manuscript

Frey, H. U., Mende, S. B., Fuselier, S. A., Immel, T. J., & stgaard, N. (2003). Proton aurora in the cusp during southward imf. *Journal of Geophysical Research: Space Physics*, *108*(A7). Retrieved from https://agupubs.onlinelibrary.wiley.com/doi/abs/10.1029/2003JA009861 doi: https://doi.org/10.1029/2003JA009861

Gérard, J.-C., Soret, L., Libert, L., Lundin, R., Stiepen, A., Radioti, A., & Bertaux, J.-L. (2015). Concurrent observations of ultraviolet aurora and energetic electron precipitation with mars express. *Journal of Geophysical Research: Space Physics*, *120*(8), 6749-6765. Retrieved from https://agupubs.onlinelibrary.wiley.com/doi/abs/10.1002/2015JA021150 doi: https://doi.org/10.1002/2015JA021150

Halekas, J., Brain, D., Lin, R., Luhmann, J., & Mitchell, D. (2008). Distribution and variability of accelerated electrons at mars. *Advances in Space Research*, *41*(9), 1347-1352. Retrieved from https://www.sciencedirect.com/science/article/pii/S0273117707000476 doi: https://doi.org/10.1016/j.asr.2007.01.034

Halekas, J., Ruhunusiri, S., Harada, Y., Collinson, G., Mitchell, D. L., Mazelle, C., ... Jakosky, B. M. (2017). Structure, dynamics, and seasonal variability of the mars-solar wind interaction: Maven solar wind ion analyzer in-flight performance and science results. *Journal of Geophysical Research: Space Physics*, *122*(1), 547-578. Retrieved from https://agupubs.onlinelibrary.wiley.com/doi/abs/10.1002/2016JA023167 doi: https://doi.org/10.1002/2016JA023167

Halekas, J. S., Brain, D. A., Luhmann, J. G., DiBraccio, G. A., Ruhunusiri, S., Harada, Y., ... Jakosky, B. M. (2017). Flows, fields, and forces in the mars-solar wind interaction. *Journal of Geophysical Research: Space Physics*, *122*(11), 11,320-11,341. Retrieved from https://agupubs.onlinelibrary.wiley.com/doi/abs/10.1002/2017JA024772 doi: https://doi.org/10.1002/2017JA024772

Halekas, J. S., Taylor, E. R., Dalton, G., Johnson, G., Curtis, D. W., McFadden, J. P., ... Jakosky, B. M. (2015, December). The Solar Wind Ion Analyzer for MAVEN. *Space Science Reviews*, *195*(1-4), 125-151. doi: 10.1007/s11214-013-0029-z

Hara, T., Seki, K., Hasegawa, H., Brain, D., Matsunaga, K., Saito, M., & Shiota, D. (2014). Formation processes of flux ropes downstream from martian crustal magnetic fields inferred from grad-shafranov reconstruction [Journal Article]. *Journal of Geophysical Research-Space Physics*, *119*(9). doi: 10.1002/2014JA019943

Harada, Y., Halekas, J., Xu, S., DiBraccio, G., Ruhunusiri, S., Hara, T., ... Mazelle, C. (2020). Ion jets within current sheets in the martian magnetosphere [Journal Article]. *Journal of Geophysical Research-Space Physics*, *125*(12). doi: 10.1029/2020JA028576

Holmberg, M. K. G., Andr, N., Garnier, P., Modolo, R., Andersson, L., Halekas, J., ... Mitchell, D. L. (2019). Maven and mex multi-instrument study of the dayside of the martian induced magnetospheric structure revealed by pressure analyses. *Journal of Geophysical Research: Space Physics*, *124*(11), 8564-8589. Retrieved from https://agupubs.onlinelibrary.wiley.com/doi/abs/10.1029/2019JA026954 doi: https://doi.org/10.1029/2019JA026954

Holsclaw, G. M., Deighan, J., Almatroushi, H., Chaffin, M., Correira, J., Evans, J. S., ... et al. (2021). The emirates mars ultraviolet spectrometer (emus) for the emm mission. *Space Science Reviews*, *217*(8). doi: 10.1007/s11214-021-00854-3

Hughes, A., Chaffin, M., Mierkiewicz, E., Deighan, J., Jain, S., Schneider, N., ... Jakosky, B. (2019). Proton aurora on mars: A dayside phenomenon pervasive in southern summer. *Journal of Geophysical Re-*

This article is protected by copyright. All rights reserved.

Author Manuscript

search: Space Physics, *124*(12), 10533-10548. Retrieved from https://agupubs.onlinelibrary.wiley.com/doi/abs/10.1029/2019JA027140 doi: https://doi.org/10.1029/2019JA027140

Jakosky, B., Lin, R., Grebowsky, J., Luhmann, J., Mitchell, D., Beutelschies, G., ... Zurek, R. (2015). The mars atmosphere and volatile evolution (maven) mission [Journal Article]. *Space Science Reviews*, *195*(1-4), 3-48. doi: 10.1007/s11214-015-0139-x

Johnston, B., Schneider, N. M., Jain, S., Milby, Z., Bowers, C., DiBraccio, G., ... Soret, L. (2023). *Discrete aurora on mars: Insights into reconnection?* Retrieved from https://doi.org/10.5194/egusphere-egu22-9415

Leblanc, F., Witasse, O., Winningham, J., Brain, J., D.A.and Lilensten, Blelly, P.-L., Frahm, R. A., ... Bertaux, J. L. (2006). Origins of the martian aurora observed by spectroscopy for investigation of characteristics of the atmosphere of mars (spicam) on board mars express. *Journal of Geophysical Research: Space Physics*, *111*(A9). Retrieved from https://agupubs.onlinelibrary.wiley.com/doi/abs/10.1029/2006JA011763 doi: https://doi.org/10.1029/2006JA011763

Lillis, R., Fillingim, M., & Brain, D. (2011). Three-dimensional structure of the martian nightside ionosphere: Predicted rates of impact ionization from mars global surveyor magnetometer and electron reflectometer measurements of precipitating electrons [Journal Article]. *Journal of Geophysical Research-Space Physics*, *116*. doi: 10.1029/2011JA016982

Lillis, R. J., Deighan, J., Brain, D., Fillingim, M., Jain, S., Chaffin, M., ... Curry, S. (2022). First synoptic images of fuv discrete aurora and discovery of sinuous aurora at mars by emm emus. *Geophysical Research Letters*, *49*(16), e2022GL099820. Retrieved from https://agupubs.onlinelibrary.wiley.com/doi/abs/10.1029/2022GL099820 doi: https://doi.org/10.1029/2022GL099820

McClintock, W., Schneider, N., Holsclaw, G., Clarke, J., Hoskins, A., Stewart, I., ... Deighan, J. (2015). The imaging ultraviolet spectrograph (iuvs) for the maven mission [Journal Article]. *Space Science Reviews*, *195*(1-4), 75-124. doi: 10.1007/s11214-014-0098-7

McGrath, M. A., Jia, X., Retherford, K., Feldman, P. D., Strobel, D. F., & Saur, J. (2013). Aurora on ganymede. *Journal of Geophysical Research: Space Physics*, *118*(5), 2043-2054. Retrieved from https://agupubs.onlinelibrary.wiley.com/doi/abs/10.1002/jgra.50122 doi: https://doi.org/10.1002/jgra.50122

Poppe, A. R., Brain, D., Dong, Y., Xu, S., & Jarvinen, R. (2021). Particle-in-cell modeling of martian magnetic cusps and their role in enhancing nightside ionospheric ion escape. *Geophysical Research Letters*, *48*(1), e2020GL090763. Retrieved from https://agupubs.onlinelibrary.wiley.com/doi/abs/10.1029/2020GL090763 (e2020GL090763 2020GL090763) doi: https://doi.org/10.1029/2020GL090763

Ruhunusiri, S., Halekas, J. S., Espley, J. R., Eparvier, F., Brain, D., Mazelle, C., ... Jakosky, B. M. (2018). An artificial neural network for inferring solar wind proxies at mars. *Geophysical Research Letters*, *45*(20), 10,855-10,865. Retrieved from https://agupubs.onlinelibrary.wiley.com/doi/abs/10.1029/2018GL079282 doi: https://doi.org/10.1029/2018GL079282

Schneider, N. M., Deighan, J. I., Jain, S. K., Stiepen, A., Stewart, A. I. F., Larson, D., ... Jakosky, B. M. (2015). Discovery of diffuse aurora on mars. *Science*, *350*(6261), aad0313. Retrieved from https://www.science.org/doi/abs/10.1126/science.aad0313 doi: 10.1126/science.aad0313

Schneider, N. M., Jain, S. K., Deighan, J., Nasr, C. R., Brain, D., Larson, D., ... Jakosky, B. M. (2018). Global aurora on mars during the september 2017 space weather event. *Geophysical Research Letters*, *45*(15), 7391-7398.

This article is protected by copyright. All rights reserved.

Author Manuscript

Retrieved from https://agupubs.onlinelibrary.wiley.com/doi/abs/10.1029/2018GL077772 doi: https://doi.org/10.1029/2018GL077772

Schneider, N. M., Milby, Z., Jain, S. K., Grard, J.-C., Soret, L., Brain, D., ... Jakosky, B. M. (2021). Discrete aurora on mars: Insights into their distribution and activity from maven/iuvs observations. *Journal of Geophysical Research: Space Physics*, *126*(10), e2021JA029428. Retrieved from https://agupubs.onlinelibrary.wiley.com/doi/abs/10.1029/2021JA029428 doi: https://doi.org/10.1029/2021JA029428

Soret, L., Grard, J.-C., Libert, L., Shematovich, V. I., Bisikalo, D. V., Stiepen, A., & Bertaux, J.-L. (2016). Spicam observations and modeling of mars aurorae. *Icarus*, *264*, 398-406. Retrieved from https://www.sciencedirect.com/science/article/pii/S0019103515004285 doi: https://doi.org/10.1016/j.icarus.2015.09.023

Soret, L., Grard, J.-C., Schneider, N., Jain, S., Milby, Z., Ritter, B., ... Weber, T. (2021). Discrete aurora on mars: Spectral properties, vertical profiles, and electron energies. *Journal of Geophysical Research: Space Physics*, *126*(10), e2021JA029495. Retrieved from https://agupubs.onlinelibrary.wiley.com/doi/abs/10.1029/2021JA029495 doi: https://doi.org/10.1029/2021JA029495

Trotignon, J., Mazelle, C., Bertucci, C., & Acuna, M. (2006). Martian shock and magnetic pile-up boundary positions and shapes determined from the phobos 2 and mars global surveyor data sets [Journal Article]. *Planetary and Space Science*, *54*(4), 357-369. doi: 10.1016/j.pss.2006.01.003

Weber, T. (2020). *The role of crustal magnetic fields in atmospheric escape from mars* (Doctoral dissertation, University of Colorado). Retrieved from https://scholar.colorado.edu/concern/graduate_thesis_or_dissertations/1544bq39m

Weber, T., Brain, D., Xu, S., Mitchell, D., Espley, J., Halekas, J., ... Jakosky, B. (2020). The influence of interplanetary magnetic field direction on martian crustal magnetic field topology. *Geophysical Research Letters*, *47*(19), e2020GL087757. Retrieved from https://agupubs.onlinelibrary.wiley.com/doi/abs/10.1029/2020GL087757 doi: https://doi.org/10.1029/2020GL087757

Weber, T., Brain, D., D.A.and Mitchell, Xu, S., Connerney, J., & Halekas, J. (2017). Characterization of low-altitude nightside martian magnetic topology using electron pitch angle distributions [Journal Article]. *Journal of Geophysical Research-Space Physics*, *122*(10), 9777-9789. doi: 10.1002/2017JA024491

Xu, S., Liemohn, M., & Mitchell, D. (2014). Solar wind electron precipitation into the dayside martian upper atmosphere through the cusps of strong crustal fields [Journal Article]. *Journal of Geophysical Research-Space Physics*, *119*(12). doi: 10.1002/2014JA020363

Xu, S., Mitchell, D., Liemohn, M., Fang, X., Ma, Y., Luhmann, J., ... Jakosky, B. (2017). Martian low-altitude magnetic topology deduced from maven/swea observations [Journal Article]. *Journal of Geophysical Research-Space Physics*, *122*(2), 1831-1852. doi: 10.1002/2016JA023467

Xu, S., Mitchell, D. L., McFadden, J. P., Fillingim, M. O., Andersson, L., Brain, D. A., ... Espley, J. (2020). Inverted-v electron acceleration events concurring with localized auroral observations at mars by maven. *Geophysical Research Letters*, *47*(9), e2020GL087414. Retrieved from https://agupubs.onlinelibrary.wiley.com/doi/abs/10.1029/2020GL087414 doi: https://doi.org/10.1029/2020GL087414

Xu, S., Mitchell, D. L., McFadden, J. P., Schneider, N. M., Milby, Z., Jain, S., ... Johnston, B. (2022). Empirically determined auroral electron events at mars-maven observations. *Geophysical Research Letters*, *49*(6), e2022GL097757. Retrieved from https://agupubs.onlinelibrary.wiley.com/doi/abs/

This article is protected by copyright. All rights reserved.

10.1029/2022GL097757 doi: https://doi.org/10.1029/2022GL097757

Zhang, C., Rong, Z., Klinger, L., Nilsson, H., Shi, Z., He, F., ... Wei, Y. (2022). Three-dimensional configuration of induced magnetic fields around mars. *Journal of Geophysical Research: Planets*, *127*(8), e2022JE007334. Retrieved from https://agupubs.onlinelibrary.wiley.com/doi/abs/10.1029/2022JE007334 doi: https://doi.org/10.1029/2022JE007334

Author Manuscript

This article is protected by copyright. All rights reserved.